Applied Surface Science 332 (2015) 80–88

Contents lists available at ScienceDirect

Applied Surface Science

journal homepage: www.elsevier.com/locate/apsusc

Mechanical property and wear performance dependence on processing condition for cold-sprayed WC-(nanoWC-Co)

Guan-Jun Yang[a], Pei-Hu Gao[a,b], Cheng-Xin Li[a], Chang-Jiu Li[a,*]

[a] State Key Laboratory for Mechanical Behavior of Materials, School of Materials Science and Engineering, Xi'an Jiaotong University, Xi'an, Shannxi 710049, PR China

[b] School of Materials and Chemical Engineering, Xi'an Technological University, Xi'an, Shannxi 710032, PR China

ARTICLE INFO

Article history:
Received 8 November 2014
Received in revised form
26 December 2014
Accepted 19 January 2015
Available online 27 January 2015

Keywords:
Cold spray
WC-(nanoWC-Co)
Hardness
Toughness
Wear resistance

ABSTRACT

WC-(nanoWC-Co) with micro-WC reinforcing particles in nanoWC-Co cermet matrix was cold-sprayed by using WC-Co with bimodal sized WC particles (with both micro-sized WC particles and nano-sized WC particles). The effect of spray powder property and post-spray treatment on the mechanical properties and wear performance of cold-sprayed WC-(nanoWC-Co) coating were examined in comparison to the conventional high-velocity oxy-fuel (HVOF)-sprayed WC-Co coating. Results showed that both hardness and toughness were influenced by the spray powder properties and the post-spray heat treatment. Compared to the HVOF-sprayed WC-Co coating with micro-sized WC particles, WC-(nanoWC-Co) exhibited much higher hardness and toughness and thereby much higher wear resistance. The further toughening of WC-(nanoWC-Co) by post-spray heat treatment significantly doubled the wear performance. The excellent wear resistance of WC-(nanoWC-Co) is attributed to the simultaneous strengthening and toughening effects resulting from the microstructure design of bimodal WC particle size distribution composed of both micro-sized and nano-sized WC particles.

1. Introduction

Carbide cermets are widely used as wear-resistant parts, cutting tools and rock drills in a variety of wear-resistant industrial applications [1–6]. Ceramic particle size and its distribution, as well as the content and composition of the cementing metal binder phase, play a decisive role in determining mechanical properties. The wear resistance of cermet depends on a material's resistance to penetration by abrasive particles or protruding asperities of mating material and the difficulty of material removal by fracture and plastic flow. Consequently, wear resistance is influenced by mechanical properties such as hardness (H) and fracture toughness (K_{IC}) [2,7,8], since material hardness indicates the deformation-resistant ability and fracture toughness indicates the fracture-resistant ability. Different from the abrasion of brittle materials, such as Al_2O_3 or Si_3N_4, dominated by fracture [9–11], the abrasion of WC-Co materials typically involves rounding, fragmentation, pullout of WC grains and removal of exposed binder, which suggests that the material removal process during abrasion involves both plastic deformation and fracture. Correlation studies of wear resistance with mechanical properties have led to the establishment of the relationships between the abrasive wear resistance and hardness/toughness. Abrasive wear resistance increases linearly with the increase of the product of fracture toughness and hardness in the form of $K_{IC}^{3/8}H^{1/2}$ according to Wayne's experimental equation [7] for cermet. Consequently, both hardness and toughness influence the wear resistance. Therefore, both high hardness and high toughness is of significant importance to the enhancement of wear resistance of cermet.

With the WC-Co system, hard WC particles act as the major wear-resistant constituent, while Co binder provides WC-Co with a high toughness [12]. The hardness and fracture toughness of WC-12Co bulk with WC particles in conventional micrometer size range are 1100–1500 Hv [13–17] and 11–20 MPa $m^{1/2}$, respectively [13,14,17]. With the decrease of WC particle size and cobalt content, the micro-hardness of WC-Co increases [12,14,16,18], accompanied by the decrease of fracture toughness [8,13,14,18–20]. When the carbide size is reduced to 10–100 nm, the hardness of a WC-12Co bulk reaches 1500–2000 Hv [14,16,17,21–25], while the fracture toughness is reduced to as low as 5–10 MPa $m^{1/2}$ [14,17,23–25]. Accordingly, most approaches to increase WC-Co hardness following the strength theory of cemented hard alloys generally encounter the problem involving the reduction of toughness.

* Corresponding author. Tel.: +86 29 82660970; fax: +86 29 83237910.
E-mail address: licj@mail.xjtu.edu.cn (C.-J. Li).

http://dx.doi.org/10.1016/j.apsusc.2015.01.138
0169-4332/

To simultaneously improve the hardness and toughness of cermet, diamond or cubic BN, which are harder than WC, are added into the cermet [26]. However, it is obvious that this approach cannot be widely applied due to the extremely high cost of those superhard ceramics. Therefore, the co-enhancement of hardness and toughness of WC-Co is still an important work full of challenges.

To achieve the co-enhancement of hardness and toughness, a WC-(nanoWC-Co) concept has been proposed by using bimodal-sized microstructure design in previous study [27,28]. With this microstructure design, both micro-sized WC particles and nano-sized WC particles are included. The cobalt binder with nano-sized WC particles constructs the nanostructured WC-Co matrix instead of pure cobalt in the conventional materials, in which micro-sized WC particles are distributed.

In this study, WC-(nanoWC-Co) powder with micro-sized WC strengthening particles and the nano-structured WC-Co matrix was cold-sprayed by using WC-Co with bimodal sized WC particles, and the effect of spray powder property and post-spray treatment on the mechanical properties and wear performance of cold-sprayed WC-(nanoWC-Co) was investigated in comparison to high-velocity oxy-fuel (HVOF)-sprayed WC-Co.

2. Experimental methods

2.1. Preparation of WC-Co powder with bimodal-sized WC

All the WC-based cermet powders and deposits in this study were of the same composition, i.e. 88 wt% WC and 12 wt% Co. The bimodal-sized WC particles were prepared through high-energy ball-milling and detailed information can be found in literature [27]. A commercial WC-12Co powder (8812, Xinke, Wuxi, China) containing 1–2 μm WC particles was ball-milled for different durations in a high-energy ball mill (ND4-2L, Tianzun, Nanjing, China) with a ball-to-powder weight ratio of 10:1 at a rotation speed of 220 rpm. The milling vial and milling balls were made of WC-Co in order to avoid contamination. To obtain a porous powder suitable for cold-spraying consolidation, the milled powder was cold-compacted to form a green body with different porosity followed by sintering in a hydrogen atmosphere at 1000 °C for 18 h. Then the powder in a size range from 20 to 30 μm was obtained by crushing the sintered WC-Co followed by sifting. In this study, the spray powders are abbreviated by the processing parameters, as shown in Table 1.

2.2. Deposition of WC-Co

Cold spraying was employed for the consolidation of WC-(nanoWC-Co) from the WC-(nanoWC-Co) powder using a cold-spraying system (CS-2000) which was developed in Xi'an Jiaotong University and whose installation was described in detail elsewhere [29]. The spray nozzle employed in this study was a convergent–divergent nozzle with a throat diameter of 2 mm. Helium was used as both the accelerating gas and the powder feeder gas. The gas pressure and temperature in the pre-chamber were 2 MPa and 600 °C, respectively. The standoff distance from the nozzle exit to the substrate surface was 20 mm. To further improve the carbide/binder interface adhesion, the as-consolidated WC-Co was annealed at 1000 °C for 6 h in a hydrogen atmosphere.

HVOF spraying was used to deposit (micro-WC)-Co in comparison to cold-sprayed WC-(nanoWC-Co) using a HVOF system (CH-2000) developed in Xi'an Jiaotong University. Propane (at a pressure of 0.4 MPa and a flow of 1300 L/h) and oxygen (at a pressure of 0.55 MPa and a flow of 13,000 L/h) were used to generate supersonic flame. Nitrogen gas was used as a powder feed gas. The spray distance was 180 mm. The spray powder was the same as the commercially WC-12Co powder used for the starting powder of WC-(nanoWC-Co) powder.

Table 1
Processing parameters of spray powders and porosities of four powders.

Powder type	Milling duration (h)	Powder porosity (%)
70h-P30	70	30
70h-P40	70	40
120h-P30	120	30
120h-P40	120	40

2.3. Characterization of microstructure and mechanical properties

The microstructure of WC-Co was characterized by scanning electron microscopy (SEM; VEGA II-XMU, TESCAN, Brno, Czech Republic). X-ray diffraction (XRD; XRD-6000, Shimadzu, Kyoto, Japan) was employed to characterize the phase structure. WC particle size in the cermet was measured by a laser diffraction particle size analyzer (MASTERSIZER 2000, Malvern, Worcestershire, UK). The WC particles were separated from the cermet by dissolving the cobalt binder phase into hydrochloric acid.

The micro-hardness of the WC-Co was measured by a Vickers micro-hardness tester (HV-5, Taiming, Shanghai, China) under a load of 300 g for a loading duration of 30 s. The fracture toughness was estimated by diamond pyramid (Vickers) indentation test under a load of 5000 g for a loading duration of 30 s using Niihara's equation corresponding to Pamlqvist type crack [19,30–32]. Ten measurements were carried out for each hardness or toughness.

Abrasion wear test was conducted on a pin-on-disk tribometer (ML-10, Xuanhua, Hebei, China) in ambient temperature and humidity. Coatings were deposited on the end of a pin of a size of Φ 4 × 30 mm. The test was carried out at a load of 9.8 N with WC-Co sliding against silicon carbide emery paper (300#) which was lined on the disk rotating at a speed of 60 rpm. During abrasion wear test, pin was driven to move toward the disk center at a speed of 4 mm per turn. This ensured that WC-Co was abraded by fresh emery paper during the whole test. Each sample was tested for five runs and three samples were used to obtain the mean wear weight loss.

3. Results

3.1. Microstructure of WC-(nanoWC-Co) spray powders

Fig. 1 shows the XRD patterns of WC-(nanoWC-Co) spray powders. WC and β-Co phases were detected for the powder. Typical cross-sectional microstructures of starting powder and

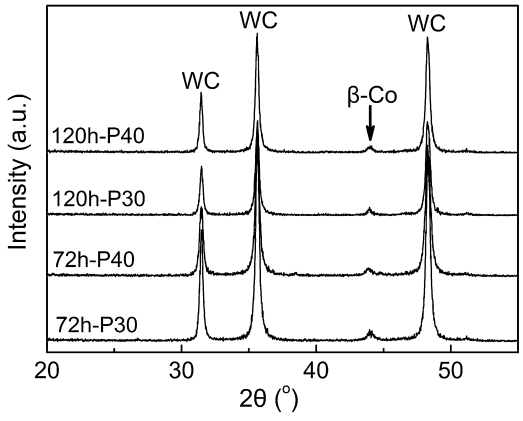

Fig. 1. XRD patterns of different spray powders.

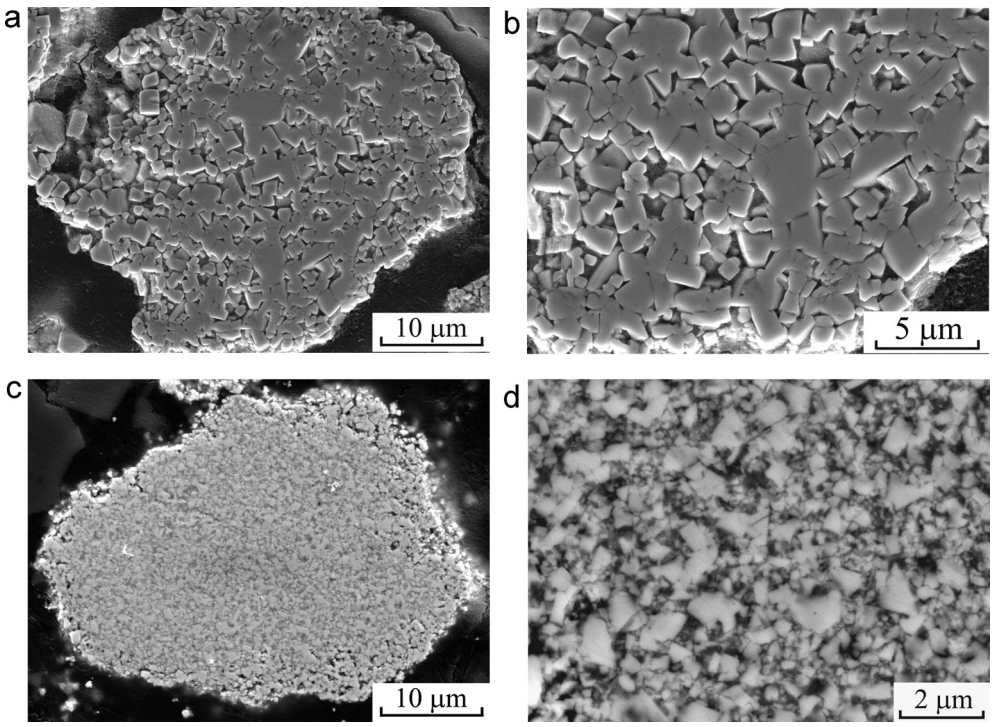

Fig. 2. Typical cross-sectional microstructure of starting powder (a, b) and 72h-P40 powder (c, d).

WC-(nanoWC-Co) spray powder are shown in Fig. 2. The WC particle size in spray powder was significantly reduced compared to the starting powder. Compared to relatively large WC particles in the starting powder (Fig. 2a and b), WC particles in the WC-(nanoWC-Co) spray powder (Fig. 2c and d) presented a bimodal size distribution, i.e. micrometer size and nanometer size. Fig. 3 further quantitatively reveals the WC particle size distribution in the WC-(nanoWC-Co) spray powder. The fraction of nano-sized WC particles (compared to all WC particles) increased from 9.5 to 12% with increasing ball milling duration from 72 to 120 h. In addition, the detailed WC particle size distribution changed a little. Considering all WC particles, the binder phase is metallic Co phase. However, if considering only micro-sized WC particles as hard reinforcement, the matrix should be the nanoWC-Co cermet which is composed of nano-sized WC particles and Co binder phase. Therefore, the spray powder with a bimodal WC particle size distribution in this study is termed as WC-(nanoWC-Co) [27].

3.2. Microstructure of WC-(nanoWC-Co) coatings

Fig. 4 shows the XRD patterns of cold-sprayed coatings using different spray powders. As expected, only WC and Co phases can be detected in all coatings. However, some β-Co phase transformed to α-Co phase during the cold spray deposition, resulting in α+β-Co dual-phase structure in the cold-sprayed coatings. This is evidently different from most reported literature on cold-sprayed WC-Co coatings [33–36]. Fig. 5 reveals the cross-sectional microstructure of cold-sprayed coatings using different spray powders. It can be found that cold-sprayed coatings presented a dense microstructure. The bimodal WC particle size distribution was well retained into deposits, forming WC-(nanoWC-Co) coatings. After annealing at 1000 °C, the α-Co phase transformed back to β-Co phase (Fig. 6). The bimodal WC particle size distribution was not influenced by the annealing treatment (Fig. 7).

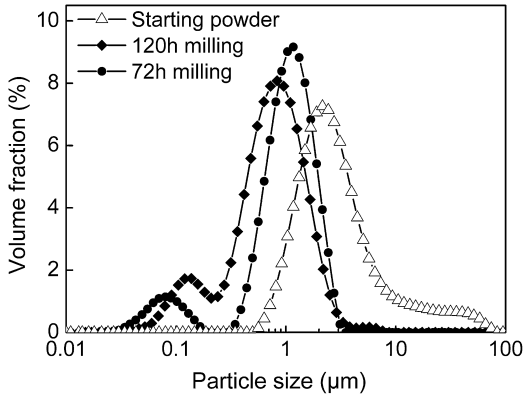

Fig. 3. WC particle size distribution (based on volume fraction) in starting powder and the powders ball milled for different durations.

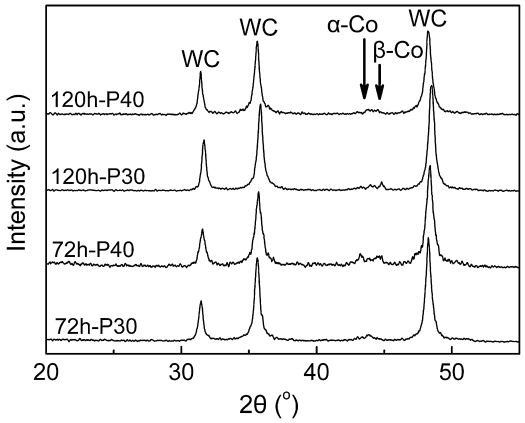

Fig. 4. XRD patterns of cold-sprayed coatings using different spray powders.

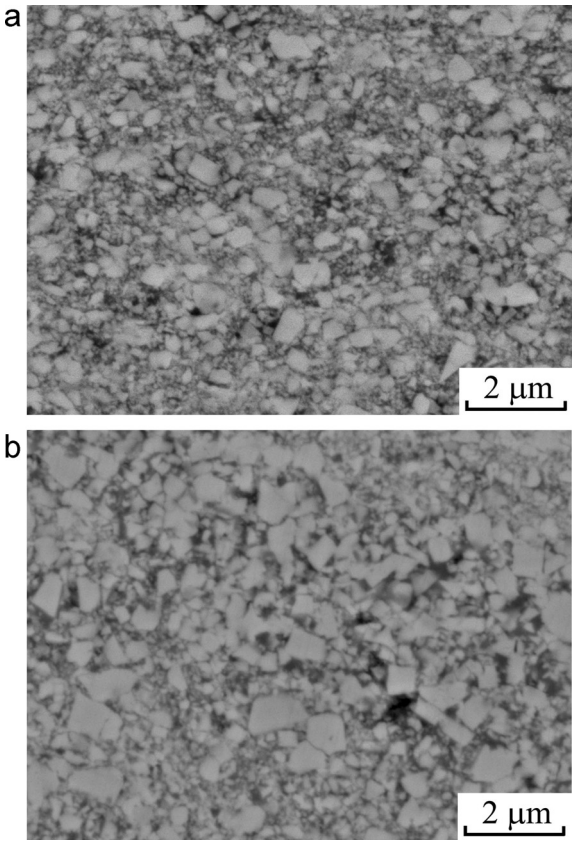

Fig. 5. Typical cross-sectional microstructure of cold-sprayed coatings using different spray powders: (a) 120h-40P; (b) 120h-30P.

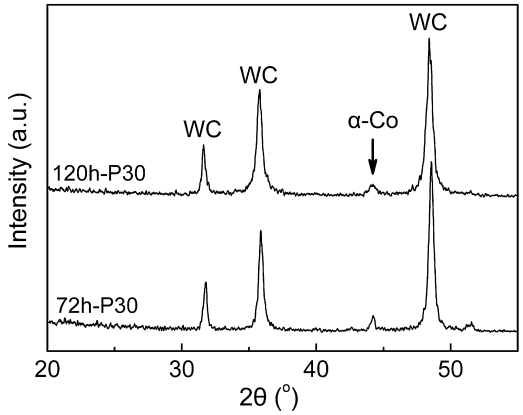

Fig. 6. XRD patterns of coatings after annealing treatment.

3.3. Mechanical properties of WC-(nanoWC-Co) coatings

Fig. 8 shows the effect of processing parameter and annealing treatment on coating hardness and toughness. It can be found from Fig. 8a that the cold-sprayed coatings presented a very high hardness of 1600–2000 Hv for different processing parameters. The increase of powder milling duration from 72 to 120 h led to a higher hardness for the cold-sprayed coating. Moreover, the lower porosity of the spray powder led to a little higher hardness for the cold-sprayed coating. After annealing treatment, the coating hardness tended to decrease a little. Compared to the typical hardness of ~1200 Hv of microWC-12Co with micro-sized WC particles [13–18], WC-(nanoWC-Co) coatings prepared in this study presented a comparable high hardness to nanoWC-12Co (~1800 Hv) [12,14,16,18,37,38]. Fig. 8b shows the effect of processing parameter and annealing treatment on coating toughness. Compared to the relatively low toughness of nanoWC-12Co with micro-sized

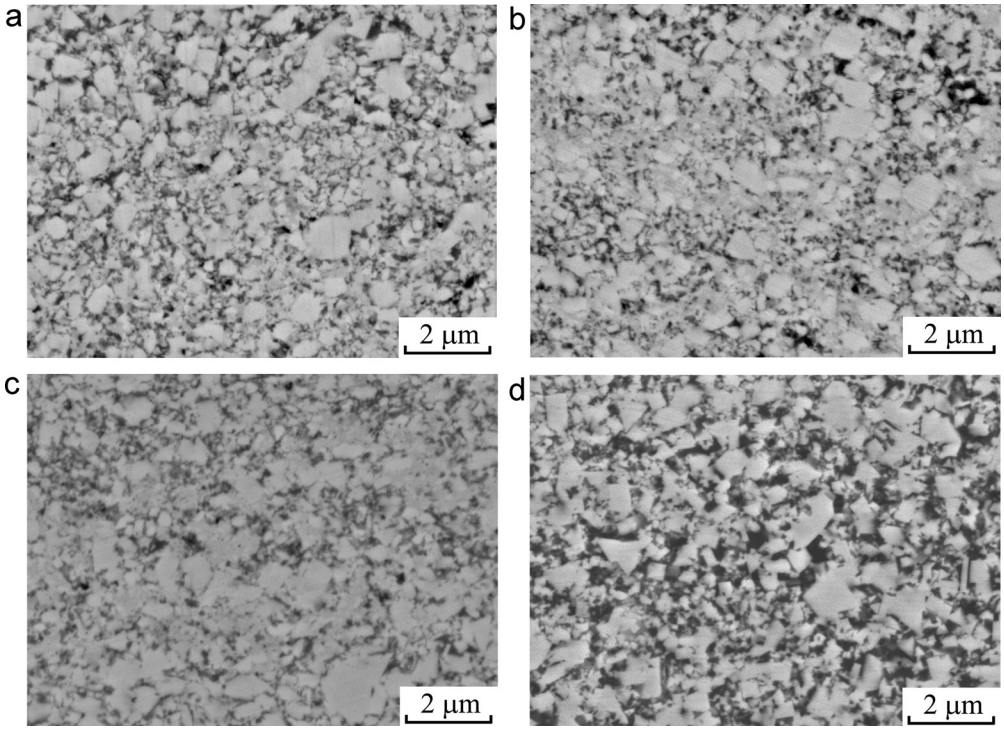

Fig. 7. Typical cross-sectional microstructure of coatings after annealing treatment: (a) 72h-40P; (b) 72h-30P; (c) 120h-40P; (d) 120h-30P.

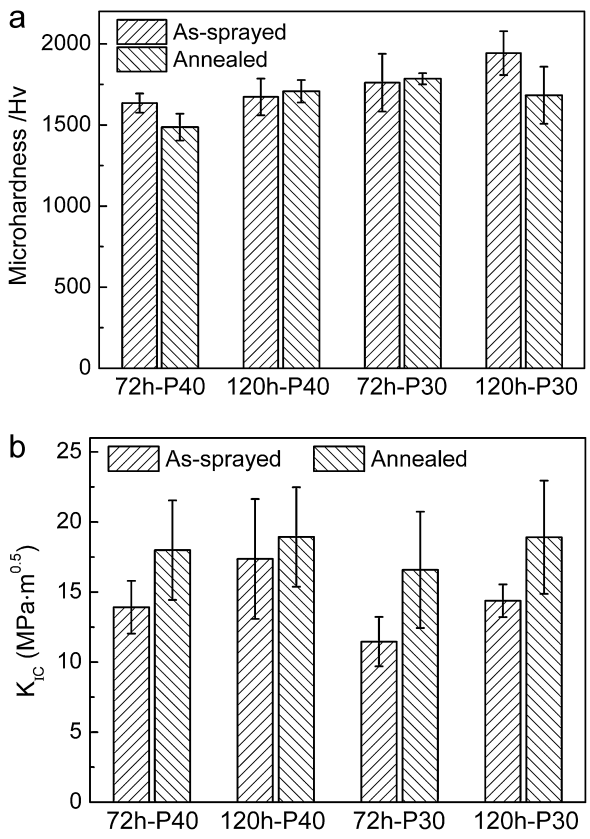

Fig. 8. Effect of processing parameter and annealing treatment on coating hardness and toughness: (a) hardness; (b) toughness.

WC particles, WC-(nanoWC-Co) coatings possessed a comparable high toughness to microWC-12Co (11–20 MPa m$^{1/2}$) [13,14,17].

3.4. Wear performance of WC-12Co coatings

Fig. 9 shows the comparison of the wear performance of cold-sprayed WC-(nanoWC-Co) coatings (120h-P30) and HVOF-sprayed microWC-12Co coatings with the same nominal constituent of WC-12Co. Compared to the HVOF-sprayed microWC-12Co coating which was widely used in various industries, the cold-sprayed WC-(nanoWC-Co) coating presented a higher wear resistance. The annealing treatment reduced the wear performance of HVOF-sprayed coatings. However, the wear resistance of the cold-sprayed WC-(nanoWC-Co) coating was significantly improved by more than one-fold.

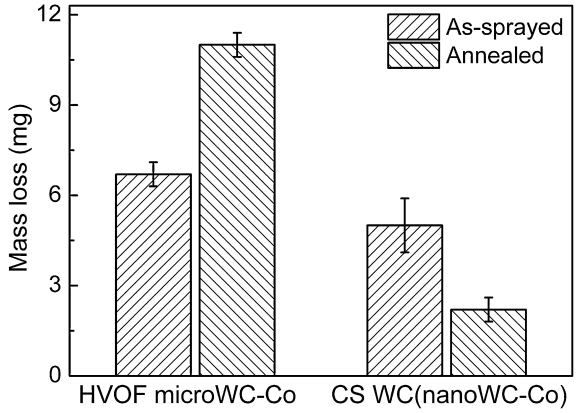

Fig. 9. The wear performance of cold-sprayed and HVOF-sprayed WC-12Co coatings.

4. Discussion

4.1. Co phase transformation during cold spraying

Results showed that the bimodal WC particle structure in spray powders is well retained into the cold-sprayed coatings. This can be attributed to the much lower processing temperature of spray powder during cold spraying than the grain coarsening temperature and even the melting temperature. It is interestingly found that Co binder phase transformation from β-Co to α-Co occurs during cold spraying. However, thermodynamically stable β-Co rather than metastable α-Co is often found in cold-sprayed WC-Co cermet coatings in literature [33–36], since close-packed hexagonal (cph) β-Co is thermodynamically stable and face-centered cubic (fcc) α-Co is metastable at room temperature. Since fcc α-Co is a metastable phase, it transforms back to cph β-Co after annealing treatment, as shown in Fig. 6.

This Co binder phase transformation from β-Co to α-Co occurred during cold-spraying would be closely related to the high-velocity impact deposition process of bimodal WC-Co powders. Although fcc α-Co is metastable at room temperature, the phase transformation from cph β-Co to fcc α-Co can be rationally promoted by the high strain rate plastic deformation as reported in literature [39–41], in which the Co binder phase undergoes very severe plastic deformation in processing approaches such as high-pressure torsion method.

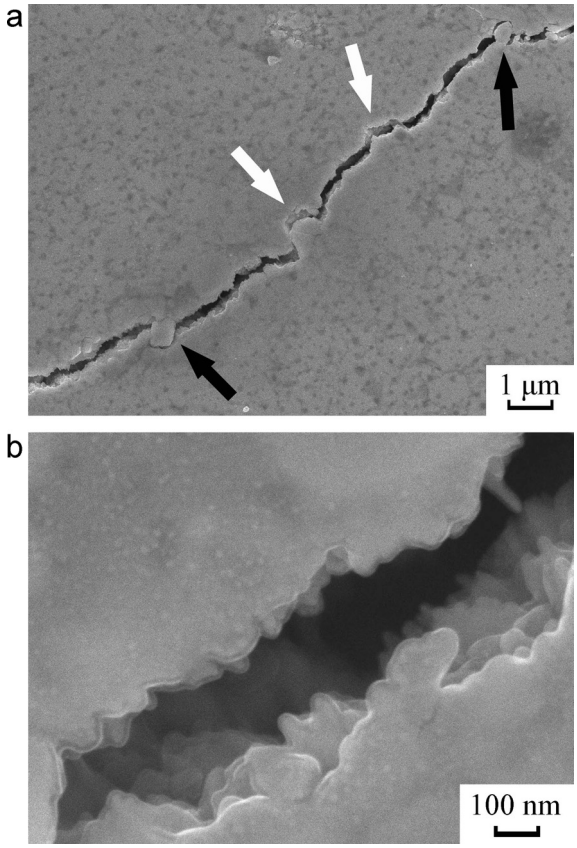

Fig. 10. Typical crack morphology in WC-(nanoWC-Co): (a) overview [27]; (b) detailed nano-zigzag.

For the cold spraying of WC-Co cermet coatings, conventional WC-Co spray powders, which are relatively dense and widely used for HVOF spraying, are quite difficult to deposit due to their high hardness and thereby low deformability. In order to enhance the deformability of spray powder, porous WC-Co powder structure design was proposed in the previous study [27,42]. The partial deformation behavior of porous particles provides the surface layer of deposited particle as the coating surface with certain deformation ability [42]. An extremely high pressure is generated during the high-velocity impact of spray powders on deposit surface or coating surface. On the one hand, the deformation of the particle results in the elimination of inter particle voids and thereby a macroscopic dense structure [42]. On the other hand, the porous structure of particle is also effectively densified at a microscopic scale due to the high pressure [27]. As a result, an overall dense microstructure is finally achieved. Similarly, a quite dense WC-(nanoWC-Co) coating is achieved by using bimodal structured WC-Co powders.

During the high-velocity impact of spray particle on deposit surface, the apparent plastic deformation of WC-Co powder would be dominated by the true plastic deformation of Co binder phase because WC particles are of extremely higher hardness than Co phase. To achieve a certain deformation of the overall WC-Co powder, Co phase must possess a much intensive true plastic deformation. In addition, the whole deformation of the WC-Co powder occurs during an extremely short duration of about dozens of nanoseconds [43,44]. As a result, the plastic deformation of Co phase has an extremely high strain rate of $\sim 3–5 \times 10^8\ s^{-1}$, which is so high that can lead to the localized amorphization of Ni-based alloy during cold spraying of cBN-NiCrAl cermet [45]. Therefore, the high strain rate plastic deformation during cold spraying promotes the Co binder phase transformation from β-Co to α-Co occurred during cold spraying.

4.2. Simultaneous strengthening and toughening effects in WC-(nanoWC-Co)

The simultaneous strengthening and toughening effects in WC-(nanoWC-Co) have been reported in previous study [27,28]. In detail, WC-(nanoWC-Co) coatings exhibit both a high hardness comparable to nanoWC-Co matrix and a high toughness comparable to microWC-Co [27,28]. The high hardness can be explained by decomposing WC-(nanoWC-Co) into different constituents, i.e. micro-sized WC particles and nanoWC-Co which can be further decomposed to nanoWC particles and Co binder phase [27]. The high toughness can be attributed to the crack bridging due to the micro-sized strengthening WC particles (marked by black arrows in Fig. 10a) and much larger cracking surface area due to the bimodal zigzag cracking path resulting from the bimodal WC particles size distribution [27]. During the fracture of WC-Co cermet, cracking mainly occurs near the WC/Co interface forming zigzag cracking surface [18,46]. For the cracking morphology of WC-(nanoWC-Co) shown in Fig. 10, except for the micro-sized zigzags as shown by white arrows in Fig. 10a, nano-sized zigzags can also be clearly identified from Fig. 10b. Fig. 11 schematically shows the hierarchical crack surface morphologies of micro-WC-Co, WC-(nanoWC-Co) and nanoWC-Co. The cracking surface area of micro-WC-Co and nanoWC-Co is comparable due to their geometry similarity. However, the cracking surface area of WC-(nanoWC-Co) is much larger than two others. Although lower toughness of nanoWC-Co than microWC-Co indicates lower specific cracking energy of the nano-zigzag cracking than micro-zigzag cracking, much larger cracking surface area of WC-(nanoWC-Co) results in its higher fracture toughness [27]. The present results further proved the validity of simultaneous strengthening and toughening effects using WC-(nanoWC-Co) structure design.

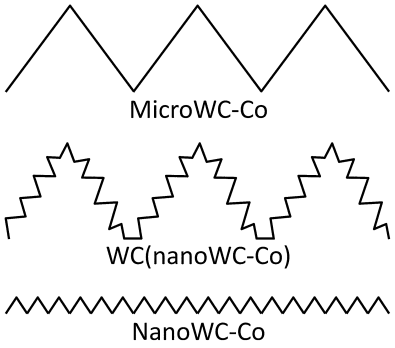

Fig. 11. Schematic diagram of crack surface morphologies of micro-WC-Co, WC-(nanoWC-Co) (bimodal) and nanoWC-Co.

4.3. Dependence of mechanical property on powder property and annealing treatment

It can be found from Figs. 7 and 8 that increasing milling duration from 72 to 120 h tends to enhance both hardness and toughness of cold-sprayed coatings. It is believed to be related to more nano-sized WC particles during longer milling duration, i.e. 12% nano-WC for 120 h milling compared to 9.5% nano-WC for 72 h milling. Fig. 2b demonstrates a near rectangular morphology of WC particles. However, the WC particles tend to change to an irregular morphology with a smaller particle size after the milling for 72 or 120 h. It means that the fracture of WC particles occur during milling treatment. From the point view of volume fraction (Fig. 3), nano-sized particles seem to be a minor fraction compared to the major fraction of micro-sized particles. However, with regard to the change in WC particle distribution based on particle number after different milling durations (Fig. 12), it can be clearly found that the number of nano-sized particles is much larger, in several orders, than that of micro-sized particles. Considering the irregular morphology of milled WC compared to the near rectangular morphology of staring WC, the nano-sized WC particles are believed to be fractured from the edge of micro-sized WC particles rather than directly separated from small WC particles. As a result, the content increase of nano-sized WC particles becomes more difficult with the milling duration, i.e. 12% for 120 h milling and 9% for 70 h milling. It is well worth to address that the fractured nano-sized WC particles would show some freshly bared surface (fracture surface), and this type of surface is of no binder phase. It is well known that the W-Co-C ternary bonding inter-layer is the most important issue for the WC-Co cermet [47]. If no ternary bonding inter-layer is formed during the following milling treatment and cold spray impact, these interfaces between WC and Co matrix would serve as pre-cracks and

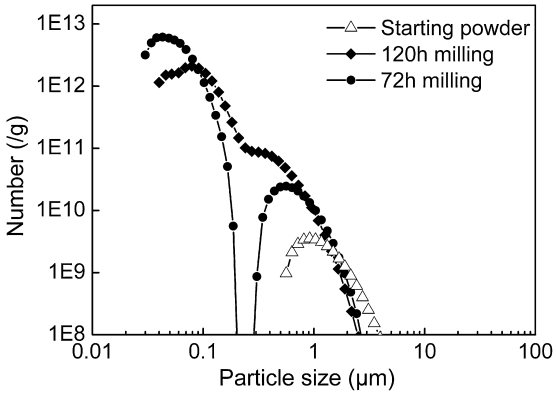

Fig. 12. WC particle size distribution (based on particle number) in starting powder and the powders ball milled for different durations.

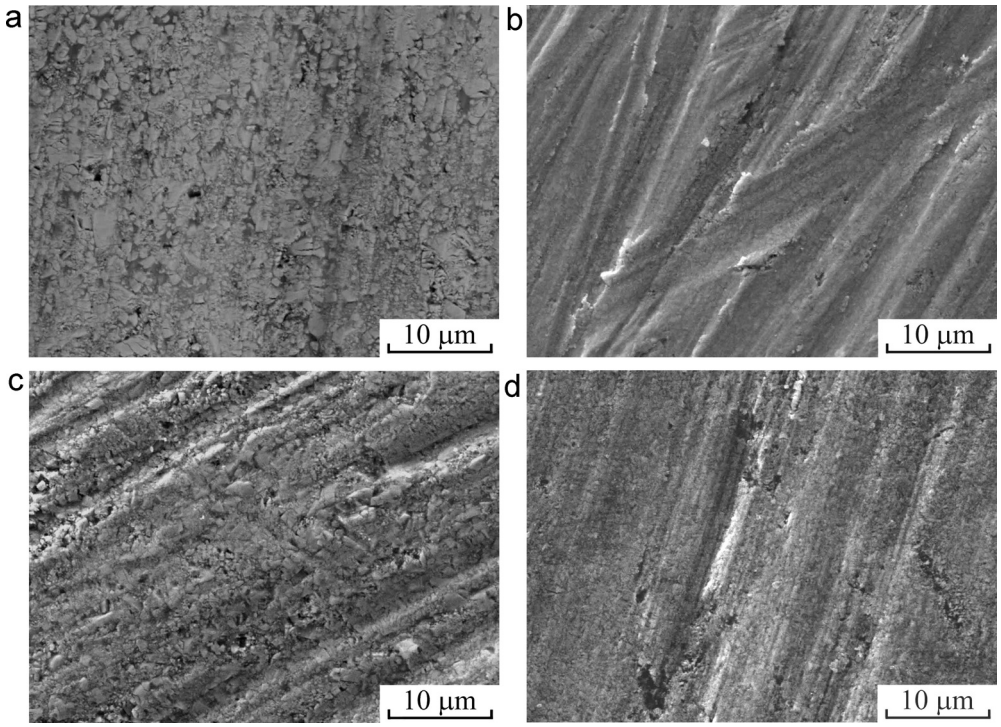

Fig. 13. Typical worn coating surface. (a) HVOF-sprayed microWC-Co; (b) cold-sprayed WC-(nanoWC-Co); (c) annealed HVOF microWC-Co; (d) annealed WC-(nanoWC-Co).

thereby limit the strength and toughness. These pre-cracks have to be healed up possibly during high-velocity impact or post-spray treatment.

It can be clearly found that the dense microstructure of WC-(nanoWC-Co) is produced by using two types of spray powders with a porosity of 30 or 40%. As discussed in Section 4.1, the intensive plastic deformation of spray powder is a necesarry condition for the succesive deposition of spray powder during cold spraying [22,36,43]. For those metallic materials with a relatively low hardness, the critical particle velocity for the cold spray deposition is generally in a range from ~250 to ~700 m/s [48,49]. However, for the WC-Co materials with a dense structure and a relatively high hardness, the cirtical velocity was reported to be as high as 800–1000 m/s [22]. In order to reduce the particle velocity and thereby reduce the processing cost, porous WC-Co powders with a relatively low hardness was proposed for the cold spraying deposition [27,42]. During the impact of a cermet powder, there is an intensive deformation near the interface between this powder and the deposition surface, which is actually a previously deposited cermet [43]. However, the powder top part, which serves as the deposit surface for the sequential deposition of spray powder, does not experience an intensive deformation and thereby retains a relatively porous structure. It would contribute to the effective deformation of this deposit surface during the sequential powder impact deposition. Therefore, two types of spray powders with a porosity of 30 or 40% result in the dense microstructure of WC-(nanoWC-Co). It should be noted that the microstructure of cold-sprayed WC-(nanoWC-Co) would also be densified by the tamping effect during the sequential impact deposition, which has been widely reported in literature [29,50].

Besides the densification of porous spray powders during cold spraying, it is worth to discuss the deformation behavior of cermet powders. It can be found that the WC particle size is not changed by the high-velocity impact of spray powder. It means that the fracture of the micro-sized and nano-zied WC particles does not occur, although it is reported that the large ceramic particles with a size of tens of micrometers are fractured during cold spraying [51–53]. It can be concluded that the deformation of the WC-(nanoWC-Co) spray powder is actually an apparent plastic deformation, which has been discussed in Section 4.1. In other words, the true plastic deformation only occurs to the metallic Co binder phase, while the possible rotation and movement of WC particles also contribute to the apparent deformation of WC-(nanoWC-Co) spray powder. As a result, the apparent deformation mainly depends on the extremely the high strain rate plastic deformation of Co binder phase. The high strain rate plastic deformation of metals produces a large number of dislocations and other crystal defects as well [54,55]. These crystal defects would increase the coating hardness via cold work hardening effect. Therefore, this is a partial hardening mechanism of cold-sprayed WC-(nanoWC-Co) in this study.

Annealing treatment tends to decrease coating hardness while evidently increases coating toughness. This can be correlated to the change of crystal defects and ineffectively bonded WC/Co interfaces. The ineffectively bonded WC/Co interfaces would be healed up during annealing treatment. This means that the healing up of pre-cracks in the WC-(nanoWC-Co) contributes to increase both hardness and toughness. The crystal defects produced by intensive plastic deformation of Co would disappear during annealing treatment at 1000 °C, which is higher than 0.2–0.4 melting point of Co metal [54,56]. This would lead to the decrease in coating hardness by eliminating the cold work hardening effect. At the same time, the disappearance of these crystal defects evidently contributes to the increase in the fracture toughness of Co binder phase. As a result, a higher toughness of WC-(nanoWC-Co) is realized after annealing treatment.

4.4. Strengthening mechanism of wear performance

Compared to widely industrialized HVOF-sprayed microWC-Co coatings, cold-sprayed WC-(nanoWC-Co) coatings present a much higher wear resistance. To reveal the enhancement mechanism of wear performance, the worn coating surface was observed and shown in Fig. 13. It can be found from Fig. 13a and c that both as-sprayed and annealed HVOF microWC-12Co coatings present a

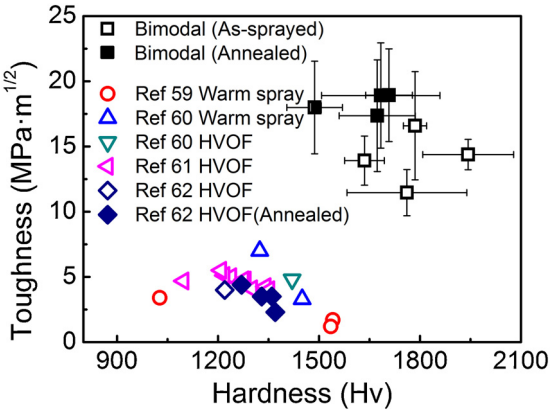

Fig. 14. Comparison of hardness and toughness of cold-sprayed WC-(nanoWC-Co) and HVOF-sprayed WC-Co.

micro-cutting weight loss mechanism. Due to the decomposition of WC particles and appearance of η phase during the annealing treatment of HVOF-sprayed microWC-Co coating, the annealing treatment leads to a decrease of wear performance [57,58]. From this point of view, the cutting weight loss of WC-(nanoWC-Co) coatings would lower than microWC-Co coating owing to a higher hardness. In addition, both cold-sprayed and annealed WC-(nanoWC-Co) coating exhibit some plastic deformation of materials as shown by the wear lips in Fig. 13b and d, since WC-(nanoWC-Co) coatings possess a relatively high toughness. Compared with as-sprayed WC-(nanoWC-Co) coating, the annealed WC-(nanoWC-Co) coating exhibits a lower hardness but a higher toughness. Consequently, annealing treatment results in an increase in wear performance for WC-(nanoWC-Co) coating. These results clearly suggest that, besides hardening effect, the toughening of WC-Co coatings is also essential to realize better wear performance.

By quantitative comparison, it can be found from Fig. 9 that the wear resistance of cold-sprayed WC-(nanoWC-Co) increases by more than double by the annealing treatment, although the fracture toughness exhibits only an increase from 14.4 to 18.9 MPa $m^{1/2}$. It is worth to further discuss the influence of microstructure evolution during annealing treatment on the wear performance of cold-sprayed WC-(nanoWC-Co). Firstly, as discussed in Section 4.3, the generation of nano-sized WC particles by mainly the edge fracture of micro-sized WC particles is accompanied with some bared WC surface without the effective W-Co-C ternary bonding inter-layer. During the cold-spraying process, the extremely short duration and relatively low temperature cannot generate the effective W-Co-C ternary bonding inter-layer. This would leave some pre-cracks in the as-sprayed cermet. Secondly, the significant apparent deformation of spray powder might result in some fracture in Co phase, if the movement or rotation of irregular hard WC particles cannot fulfill the apparent deformation of the overall spray powder. This can be similar to the micro-cracks in the deformed cermet materials and result in another form of pre-cracks in the as-sprayed cermet despite the apparent dense microstructure shown in cross-sections. During the post-spray annealing treatment, all these pre-cracks would be healed up. In addition, the crystal defects in Co binder phase induced by high-velocity impact would disappear during the annealing treatment. All these changes in the microstructure would contribute to a much higher wear performance after post-spraying annealing treatment.

To further compare the WC-(nanoWC-Co) in this study with HVOF-sprayed WC-Co, both the hardness and toughness of two types of coatings are shown in Fig. 14 (the data comes from both this study and literature). Compared to the HVOF-sprayed WC-Co coatings (and even newly developed warm sprayed coatings) [59–62], the cold-sprayed WC-(nanoWC-Co) presents obvious higher hardness and toughness. For the cold-sprayed WC-(nanoWC-Co), the further increase in toughness during heat treatment contributes to a higher wear resistance, although the hardness tends to decrease a little. However, for HVOF-sprayed coatings, the heat treatment decreases the toughness and thereby leads to a lower wear resistance, which is consistent with literature [62].

5. Conclusions

WC-(nanoWC-Co) with micro-sized WC reinforcing particles and the nano-structured WC-Co matrix was cold-sprayed by using WC-Co with bimodal-sized WC particles, and effect of powder property and post-spray treatment on the mechanical properties and wear performance was investigated. The high-velocity impact of spray powders and the relatively high transformation ability of porous WC-(nanoWC-Co) powders resulted in a dense structure. The increase in powder milling duration from 72 to 120 h enhanced both the hardness and toughness of cold-sprayed coatings due to the more nano-sized WC particles during longer milling duration. The wear performance was significantly improved by the simultaneous strengthening and toughening effects of WC-(nanoWC-Co), compared to the HVOF-sprayed WC-Co with micro-sized WC particles. Despite a little decrease in hardness, the post-spray annealing treatment of the as-sprayed WC-(nanoWC-Co) led to an increase in toughness, thereby doubling the wear resistance for the cold-sprayed WC-(NanoWC-Co).

Acknowledgements

This work is supported by the National Natural Science Foundation of China (No. 50725101) and National Program for Support of Top-notch Young Professionals.

References

[1] T.W. Gustafson, P.C. Panda, G. Song, R. Raj, Acta Mater. 45 (1997) 1633–1643.
[2] D.A. Stewart, P.H. Shipway, D.G. McCartney, Acta Mater. 48 (2000) 1593–1604.
[3] A. Petersson, J. Agren, Acta Mater. 52 (2004) 1847–1858.
[4] P.S. Babu, B. Basu, G. Sundararajan, Acta Mater. 56 (2008) 5012–5026.
[5] K.P. Mingard, B. Roebuck, J. Marshall, G. Sweetman, Acta Mater. 59 (2011) 2277–2290.
[6] C.J. Li, G.J. Yang, Int. J. Refract. Met. Hard Mater. 39 (2013) 2–17.
[7] S.F. Wayne, J.G. Baldoni, S.T. Buljan, Tribol. Trans. 33 (1990) 611–617.
[8] Q.Q. Yang, T. Senda, A. Ohmori, Wear 254 (2003) 23–34.
[9] A.G. Evans, T.R. Wilshaw, Acta Metall. 24 (1976) 939–956.
[10] J.G. Baldoni, S.F. Wayne, S.T. Buljan, ASLE Trans. 29 (1986) 347–352.
[11] A. Tewari, B. Basu, R.K. Bordia, Acta Mater. 57 (2009) 2080–2087.
[12] B. Roebuck, Int. J. Refract. Met. Hard Mater. 24 (2006) 101–108.
[13] R. Porat, J. Malek, Mater. Sci. Eng. A 105 (1988) 289–292.
[14] V. Richter, M. Von Ruthendorf, Int. J. Refract. Met. Hard Mater. 17 (1999) 141–152.
[15] S. Luyckx, A. Love, Int. J. Refract. Met. Hard Mater. 24 (2006) 75–79.
[16] S. Luyckx, N. Sacks, A. Love, Int. J. Refract. Met. Hard Mater. 25 (2007) 57–61.
[17] D. Sivaprahasam, S.B. Chandrasekar, R. Sundaresan, Int. J. Refract. Met. Hard Mater. 25 (2007) 144–152.
[18] K. Jia, T.E. Fischer, B. Gallois, Nanostruct. Mater. 10 (1998) 875–891.
[19] J.L. Chermant, F. Osterstock, J. Mater. Sci. 11 (1976) 1939–1951.
[20] Z.Z. Fang, X. Wang, T. Ryu, K.S. Hwang, H.Y. Sohn, Int. J. Refract. Met. Hard Mater. 27 (2009) 288–299.
[21] H.J. Kim, C.H. Lee, S.Y. Hwang, Mater. Sci. Eng. A 391 (2005) 243–248.
[22] C.J. Li, G.J. Yang, P.H. Gao, J. Ma, Y.Y. Wang, C.X. Li, J. Therm. Spray Technol. 16 (2007) 1011–1020.
[23] A. Michalski, D. Siemiaszko, Int. J. Refract. Met. Hard Mater. 25 (2007) 153–158.
[24] F.A. Deorsola, D. Vallauri, G.A.O. Villalba, B. De Benedetti, Int. J. Refract. Met. Hard Mater. 28 (2010) 254–259.
[25] V. Bonache, M.D. Salvador, D. Busquets, P. Burguete, E. Martinez, F. Sapina, E. Sanchez, Int. J. Refract. Met. Hard Mater. 29 (2011) 78–84.
[26] Z.Z. Fang, A. Griffo, B. White, G. Lockwood, D. Belnap, G. Hilmas, J. Bitler, Int. J. Refract. Met. Hard Mater. 19 (2001) 453–459.
[27] G.J. Yang, P.H. Gao, C.X. Li, C.J. Li, Scr. Mater. 66 (2012) 777–780.
[28] G.C. Ji, H.T. Wang, X. Chen, X.B. Bai, Z.X. Dong, F.G. Yang, Surf. Coat. Technol. 235 (2013) 536–543.

[29] C.J. Li, W.Y. Li, Surf. Coat. Technol. 167 (2003) 278–283.
[30] K. Niihara, R. Morena, D.P.H. Hasselman, J. Mater. Sci. Lett. 1 (1982) 13–16.
[31] D.B. Marshall, T. Noma, A.G. Evans, J. Am. Ceram. Soc. 65 (1982) C175–C176.
[32] M.M. Lima, C. Godoy, J.C. Avelar-Batista, P.J. Modenesi, Mater. Sci. Eng. A 357 (2003) 337–345.
[33] M. Couto, S. Dosta, M. Torrell, J. Fernandez, J.M. Guilemany, Surf. Coat. Technol. 235 (2013) 54–61.
[34] M. Yandouzi, E. Sansoucy, L. Ajdelsztajn, B. Jodoin, Surf. Coat. Technol. 202 (2007) 382–390.
[35] S. Dosta, M. Couto, J.M. Guilemany, Acta Mater. 61 (2013) 643–652.
[36] R.S. Lima, J. Karthikeyan, C.M. Kay, J. Lindemann, C.C. Berndt, Thin Solid Films 416 (2002) 129–135.
[37] K. Jia, T.E. Fischer, Wear 200 (1996) 206–214.
[38] K. Jia, T.E. Fischer, Wear 203 (1997) 310–318.
[39] E. Menendez, J. Sort, S. Surinach, M.D. Baro, J. Nogues, J. Mater. Res. 22 (2007) 2998–3005.
[40] E. Menendez, J. Sort, V. Langlais, A. Zhilyaev, J.S. Munoz, S. Surinach, J. Nogues, M.D. Baro, J. Alloys Compd. 434 (2007) 505–508.
[41] J. Sort, A. Zhilyaev, M. Zielinska, J. Nogues, S. Surinach, J. Thibault, M.D. Baro, Acta Mater. 51 (2003) 6385–6393.
[42] P.H. Gao, Y.G. Li, C.J. Li, G.J. Yang, C.X. Li, J. Therm. Spray Technol. 17 (2008) 742–749.
[43] T. Schmidt, F. Gartner, H. Assadi, H. Kreye, Acta Mater. 54 (2006) 729–742.
[44] H. Assadi, F. Gartner, T. Stoltenhoff, H. Kreye, Acta Mater. 51 (2003) 4379–4394.
[45] X.T. Luo, G.J. Yang, C.J. Li, K. Kondoh, Scr. Mater. 65 (2011) 581–584.
[46] H.C. Kim, D.Y. Oh, I.J. Shon, Int. J. Refract. Met. Hard Mater. 22 (2004) 197–203.
[47] A.S. Kurlov, A.I. Gusev, A.A. Rempel, Int. J. Refract. Met. Hard Mater. 29 (2011) 221–231.
[48] C.J. Li, W.Y. Li, Y.Y. Wang, G.J. Yang, H. Fukanuma, Thin Solid Films 489 (2005) 79–85.
[49] C.J. Li, H.T. Wang, Q. Zhang, G.J. Yang, W.Y. Li, H.L. Liao, J. Therm. Spray Technol. 19 (1–2) (2010) 95–101.
[50] Y.M. Xiong, G. Bae, X. Xiong, C. Lee, J. Therm. Spray Technol. 19 (2010) 575–585.
[51] A.S.M. Ang, C.C. Berndt, P. Cheang, Surf. Coat. Technol. 205 (2011) 3260–3267.
[52] X.K. Suo, Q.L. Suo, W.Y. Li, M.P. Planche, H.L. Liao, J. Therm. Spray Technol. 23 (2014) 91–97.
[53] M. Yu, X.K. Suo, W.Y. Li, Y.Y. Wang, H.L. Liao, Appl. Surf. Sci. 289 (2014) 188–196.
[54] C. Borchers, F. Gartner, T. Stoltenhoff, H. Kreye, Acta Mater. 53 (2005) 2991–3000.
[55] X.T. Luo, G.J. Yang, C.J. Li, Surf. Coat. Technol. 205 (2011) 4808–4813.
[56] X.T. Luo, C.J. Li, J. Therm. Spray Technol. 21 (2012) 578–585.
[57] Q. Wang, L.X. Li, G.B. Yang, X.Q. Zhao, Z.X. Ding, Surf. Coat. Technol. 206 (2012) 4000–4010.
[58] S.K. Asl, M.H. Sohi, K. Hokamoto, M. Uemura, Wear 260 (2006) 1203–1208.
[59] P. Chivavibul, M. Watanabe, S. Kuroda, J. Kawakita, M. Komatsu, K. Sato, J. Kitamura, J. Therm. Spray Technol. 20 (2011) 1098–1109.
[60] P. Chivavibul, M. Watanabe, S. Kuroda, J. Kawakita, M. Komatsu, K. Sato, J. Kitamura, J. Therm. Spray Technol. 19 (2010) 81–88.
[61] Q. Wang, Z. Chen, L. Li, G. Yang, Surf. Coat. Technol. 206 (2012) 2233–2241.
[62] Q. Wang, L. Li, G. Yang, X. Zhao, Z. Ding, Surf. Coat. Technol. 206 (2012) 4000–4010.